12

EDGEWOOD
RESEARCH, DEVELOPMENT & ENGINEERING CENTER
U.S. ARMY CHEMICAL AND BIOLOGICAL DEFENSE COMMAND

ERDEC-TR-238

MECHANISTIC STUDY OF THE EVAPORATION OF LIQUIDS FROM POROUS MICROPARTICLES

Glenn O. Rubel

RESEARCH AND TECHNOLOGY DIRECTORATE

May 1995

CUM SCIENTIA DEFENDIMUS

Aberdeen Proving Ground, MD 21010-5423

Disclaimer

The findings in this report are not to be construed as an official Department of the Army position unless so designated by other authorizing documents.

REPORT DOCUMENTATION PAGE

Form Approved
OMB No: 0704-0188

1. AGENCY USE ONLY *(Leave blank)*	2. REPORT DATE	3. REPORT TYPE AND DATES COVERED
	1995 May	Final, 94 Jan - 95 Jan

4. TITLE AND SUBTITLE
Mechanistic Study of the Evaporation of Liquids from Porous Microparticles

5. FUNDING NUMBERS
PR-1O161102A71A

6. AUTHOR(S)
Rubel, Glenn O.

7. PERFORMING ORGANIZATION NAME(S) AND ADDRESS(ES)
DIR, ERDEC, ATTN: SCBRD-RTE, APG, MD 21010-5423

8. PERFORMING ORGANIZATION REPORT NUMBER
ERDEC-TR-238

9. SPONSORING / MONITORING AGENCY NAME(S) AND ADDRESS(ES)

10. SPONSORING / MONITORING AGENCY REPORT NUMBER

11. SUPPLEMENTARY NOTES

12a. DISTRIBUTION / AVAILABILITY STATEMENT
Approved for public release; distribution is unlimited.

12b. DISTRIBUTION CODE

13. ABSTRACT *(Maximum 200 words)*

The objective of this study is to investigate the evaporation of volatile liquids from individual microparticles composed of an aggregate of primary porous particles. The evaporation of octyl alcohol from microparticles containing porous silica was measured using single particle electrodynamic levitation. Liquid evaporation rates were determined from changes in the particle-levitation electric field intensities. A class of Syloid silicas was chosen for this study because of their well-defined pore volumes and specific surface areas which both affect the liquid evaporation rate. It is shown that the silica matrix retards octyl alcohol evaporation, and the degree of evaporation retardation increases with decreasing silica pore radius. A shrinking core evaporation model is used to interpret experimental results, and pore radii are determined for each of the silicas. This study also demonstrates that single particle levitation can be used to determine the liquid absorption capacity of solid particles.

14. SUBJECT TERMS
Porosity
Pore radius
Evaporation
Microparticles
Particle levitation

15. NUMBER OF PAGES
29

16. PRICE CODE

17. SECURITY CLASSIFICATION OF REPORT	18. SECURITY CLASSIFICATION OF THIS PAGE	19. SECURITY CLASSIFICATION OF ABSTRACT	20. LIMITATION OF ABSTRACT
UNCLASSIFIED	UNCLASSIFIED	UNCLASSIFIED	UL

Blank

PREFACE

The work described in this report was authorized under Project No. 1O161102A71A, Research in CW/CB Defense. This work was started in January 1994 and completed in January 1995.

The use of trade or manufacturers' names in this report does not constitute an official endorsement of any commercial products. This report may not be cited for advertisement purposes.

This report has been approved for public release. Registered users should request additional copies from the Defense Technical Information Center; unregistered users should direct such requests to the National Technical Information Service.

Acknowledgments

This author would like to extend thanks to W.R. Grace Chemical Company for providing the Syloid silicas and related physical/chemical property data.

Blank

CONTENTS

FIGURES

TABLE

MECHANISTIC STUDY OF THE EVAPORATION OF LIQUIDS FROM POROUS MICROPARTICLES

Introduction

An understanding of the evaporation of hazardous liquids from porous solids is critical to developing accurate hazard assessments of liquid spills. While considerable work has been conducted on the evaporation of liquids from solid beds, less attention has been directed to understanding mass transfer from the individual microparticles constituting the solid. Abramzon et al. (1973) conducted a theoretical analysis on the drying time of porous particles in a fluidized bed.

In this study experimental evidence is presented that the evaporation of liquids from microparticles composed of porous material can be effected by the pore dimensions of the solid. In the present study the evaporation of octyl alcohol from porous silica aggregate microparticles is measured. A class of Syloid silica, commercially produced by W.R. Grace Chemical Company, is used in this study because of its well defined porosity (see Table 1). The microparticles in this study vary in diameter from 100 to 150 micrometers and the primary particle size of the silicas vary from 3 to 9 micrometers in diameter. Thus the experimental evaporation rates correspond to the evaporation of octyl alcohol from an aggregate of silica particles.

The experimental system used to study microparticle evaporation is referred to as the single particle electrodynamic levitater (SPEL). SPEL is an ultrasensitive gravimetric method which uses levitating electric fields to detect the weight change of individual particles. The sensitivity of the system is such that weight changes on the order of tens of nanograms can be detected with this system. An added feature of this unit is, that by working with microparticles 100 micrometers in diameter, telemicroscopy can be used to monitor morphology changes in the particle, vis-a`-vis, wet and solid particles. This capability is important when correlating the liquid evaporation rate to the physical state of the microparticle.

Phenomenologically, the evaporation of liquids from porous solids is controlled by evaporation from the interstitial volume of the bulk solid (interparticle) and evaporation from the pores of the individual microparticles constituting the solid (intraparticle). In this study, interstitial evaporation is neglected and evaporation is assumed to be controlled by evaporation through the pores. A shrinking core evaporation model (Rubel, 1987) is developed and used to compare experiment and theory. The shrinking core model assumes that the liquid evaporates through an ever-thickening porous shell which is parameterized by an effective diffusion coefficient. The effective diffusion coefficient depends on, among other things, the shell pore radius. Rubel (1987) showed that for ammonia gas diffusing through an ammonium phosphate

shell, the rate of gas diffusion decreased as the pore size decreased. By comparing theory to experiment, the effective diffusion coefficient for the silica is determined. Using Wheeler's (1955) parallel pore model in combination with capillary diffusion theory, the effective pore radius of the silica is determined and compared to literature values.

Experimentation

A schematic of the particle trap and ancillary equipment is shown in Figure 1. The particle trap consists of a central electrode in the shape of a hyperboloid of revolution over which an oscillating potential is applied. This electrode geometry establishes an electric field which produces a net time-averaged force on a charged particle causing the particle to execute bounded oscillatory motion. Superimposed on the oscillating electric field is a static field created by two endcap electrodes oriented such that the static electric field force counterbalances the gravitational force on the particle. A.C. current voltages typically vary between 500 and 1000 volts and D.C. current voltages vary between 0 and 200 volts.

The D.C. voltage is adjusted until the trapped particle ceases oscillatory motion and comes to rest at the focal plane of the telemicroscope. Under this condition, the electric force equals the gravitational force and the particle mass can be determined. The telemicroscope is equipped with a scanning graticule that permits particle diameter measurements to an accuracy of $\pm$ 5%. Automatic positioning of the particle is achieved using a servo-mechanism. The servo uses a split photodiode detector to measure laser light scattered in the forward direction. If the particle migrates from the trap center, an error signal is generated that is converted to a correction voltage that repositions the particle at the center of the trap.

The silica-octyl alcohol mixture particles are prepared by adding a sufficient quantity of alcohol to the powder silica until the mixture attains a liquid consistency. In some experiments the silica was preheated for one hour at an oven temperature of 150°C and one atmosphere pressure to desorb preexisting water vapor. However, evaporation experiments showed no difference between preheated and unheated silica samples. The mixture is stirred and allowed to stand for a period of one hour. After this period of time, the mixture is drawn into a pipette in which a conducting wire is immersed. Applying a critical voltage of 7KV, a spray of charged colloidal droplets is generated. If more than one droplet is captured in the cell, a glass rod is used to remove all particles except one. For the water vapor adsorption measurements, methanol-silica mixtures were prepared in the same manner as the octyl alcohol-silica mixtures. Methanol has sufficient volatility so that the electrospray-generated particles would be dry when captured in the cell. This flash evaporation method eliminated the possibility of solvent interference on water vapor adsorption.

The gas environment of the levitated particle was controlled by passing compressed air through the levitater at a flow rate of 2 cc per sec. This flow rate maintained the cell vapor free of octyl alcohol during the evaporation experiments and facilitated data analysis. The flow was

adjusted so that ventilation effects were minimized. The temperature of the cell was maintained at 25°C and all experiments were conducted at one atmosphere pressure. For the water vapor adsorption measurements, the relative humidity of the gas stream was controlled by mixing a dry air flow with a water-saturated air flow. By varying the relative flow rate of the two separate flows, a precise control of the gas dew point was achieved. The gas dew point was monitored with an EG&G dew point hygrometer.

Results and Discussion

Water Vapor Adsorption

Initial experiments focused on the measurement of the water isotherm of the silicas. Figure 2 shows the water isotherms for Syloid 63 and 244 as measured by W.R. Grace for bulk powders and as measured by the SPEL method for single micrometer-sized particles. Water loading, the ratio of the grams of water adsorbed to the grams of adsorbent, is used to quantify the degree of water adsorption. The water loading is expressed in terms of the levitation voltage according to the relation

$$\textit{Water Loading } (gm/gm) = 1 - V_D / V , \qquad (1)$$

where V_D is the levitation voltage for the dry adsorbent particle. The water loading measurements by SPEL represent the average of five separate runs, however, the reproducibility is such that the error bars are comparable to the size of the data points. Noteworthy is the close agreement between the two distinct methods of measurement, i.e., single particle and bulk adsorption. This remarkable finding suggests that SPEL can be used to measure adsorption isotherms of powders in one-tenth the time of classical methods, i.e., one hour as compared to one day. In addition, because of the small quantities of material required for the measurement, toxic material handling is minimized.

The data in Figure 2 clearly shows that Syloid 63 adsorbs more water vapor than Syloid 244 for relative humidities less than 70%. This is primarily due to the smaller pore size of Syloid 63 which results in pore condensation at the lower relative humidities. Pore condensation is the consequence of capillary filling which exhibits a concave meniscus that lowers the vapor pressure relative to a plane surface (Laplace, 1806). Then small pore condensation occurs before condensation onto the flat surfaces of the solid. It is for this reason that the water loading curve of Syloid 63 is elevated above that of Syloid 244.

In support of the pore filling hypothesis, it is noted that if one monolayer had adsorbed onto the solid silica, based on the projected area of a water molecule and the specific surface

area of the silicas as shown in Table 1., the water loading for Syloids 63 and 244 would be 0.17 and 0.08, respectively. From Figure 2 it is evident that more than one monolayer of water has adsorbed onto Syloid 63. In fact for the measured water adsorption, an equivalent of two monolayers of water would have been adsorbed at 60% relative humidity. However, for these relative humidities it is unlikely that multilayer formation is occurring. Thus it is postulated that pore condensation is most probable in this case. Also notice that for Syloid 244, the monolayer calculation is in closer agreement with the measured water loading, suggesting that pore filling is not as active in Syloid 244 as would be expected with the larger pores.

It is interesting to note that while the smaller pore-sized Syloid 63 exhibits greater water vapor adsorption at the lower relative humidities, the larger pore-sized Syloid 244 shows a greater saturation absorption efficiency (see Table 1). In fact the oil absorption efficiency of Syloid 63 is almost 5 times greater than that of Syloid 244. Thus as a general rule, the efficient vapor adsorbers are poor liquid absorbers because the greater internal surface area leads to a smaller internal volume for absorption.

Octyl Alcohol Desorption

Figures 3a-c show the normalized levitation voltage data for 3 different evaporating mixture particles with the following initial weight percent compositions: a- 38% Syloid 63, 62% octyl alcohol; b- 22% Syloid 244, 78% octyl alcohol; and c- 25% Syloid 72, 75% octyl alcohol. The initial composition is determined from the initial and final (dry) levitation voltages. Initially all particles are trapped in the levitater as wet particles with particle diameters varying between 100 and 160 micrometers. For comparison, the calculated levitation voltage of an evaporating droplet of octyl alcohol with a solid core and with the same initial droplet diameter is shown. The voltage decay rate of the pure droplet is calculated from the set of equations,

$$\frac{\dot{V}}{V_o} = \frac{\dot{m}}{m_o}\ ; \qquad \dot{m} = \frac{2\pi D_g M_w d\ (P_\infty - P_D)}{R_g T} \qquad (2)$$

where V_o and m_o are the initial voltage and mass, respectively. The mass decay rate is controlled by continuum diffusion and the external octyl alcohol partial pressure P_∞ is assumed to be zero. Due to the small latent heat of evaporation and evaporation rates, isothermal conditions prevail. It is evident from the calculations that the mixture particles evaporate like pure droplets initially. However, the mixture particle evaporation rate diverges from the pure droplet evaporation rate during the evaporation process. From telemicroscopic observations, it is observed that the divergence in the particle evaporation rates is associated with the particle transforming from the wet to the dry state.

To model the change in the particle evaporation rate, a shrinking core evaporation model is introduced (Rubel, 1987). The shrinking core model accounts for the diffusion of the octyl

alcohol vapor through the porous silica shell as the octyl alcohol liquid core shrinks. The shrinking core model assumes that the evaporating liquid forms a spherical core concentric with the solid particle surface. Evaporation of the liquid core is controlled by the diffusion of alcohol vapor through a porous shell that has been depleted of liquid by octyl alcohol evaporation. As the liquid core continues to evaporate, the shell thickness increases. The diffusion of gas through the shell depends on a variety of parameters including shell thickness and shell pore radius. We begin by developing the vapor concentration field within the porous shell. If one draws an arbitrary sphere of radius r, the surface of which lies within the porous shell, the flux through this sphere surface is given by

$$4\pi r^2 D_e \frac{\partial c_i}{\partial r} \equiv N \qquad (3)$$

where N is a constant for steady state conditions. The effective diffusion coefficient of the porous shell D_e and the octyl alcohol vapor concentration inside the shell c_i are shown explicitly. Integrating Eq.3 from R-τ to R, where τ is the thickness of the porous shell, and using the boundary conditions $c_i(R-\tau)=c^o$, where c^o is the saturation vapor concentration, N can be expressed as

$$N = \frac{4\pi D_e R\,(R-\tau)}{\tau}\left(c_i(R) - c^o\right). \qquad (4)$$

Likewise by integrating Eq.3 from R-τ to r, the radial dependence of the concentration field is expressed as

$$c_i(r) - c^o = \frac{N}{4\pi D_e}\left(\frac{1}{R-\tau} - \frac{1}{r}\right). \qquad (5)$$

Substituting Eq.4 into Eq.5, c_i is expressed explicitly as

$$c_i(r) - c^o = (c_i(R) - c^o) \left(\frac{R}{\tau} - \frac{R\,(R-\tau)}{r\,\tau} \right) . \qquad (6)$$

To determine $c_i(R)$, flux continuity across the R-sphere surface interface is invoked, i.e.,

$$4\pi R^2 D_e \frac{\partial c_i}{\partial r} \Big| R = 4\pi R^2 D_g \frac{\partial c_{ex}}{\partial r} \Big| R , \qquad (7)$$

where the external vapor concentration field c_{ex} satisfies the conditions

$$\Delta c_{ex} = 0 ; \quad c_{ex} = c_{ex}(\infty) \quad as \; r \to \infty .$$

Deriving the solution for c_{ex} as

$$c_{ex}(r) = (c_{ex}(R) - c_{ex}(\infty)) \frac{R}{r} + c_{ex}(\infty)$$

and substituting into Eq.7 along with Eq.6, c_i (R) is found to be

$$c_i\,(R) = \frac{D_e\, c^o\, (R-\tau)}{\tau \left(\dfrac{D_e\,(R-\tau)}{\tau} + D_g \right)} \qquad (8)$$

where it is assumed that $c_{ex}(\infty)=0$. Finally, substituting Eq.8 into Eq.6, the internal concentration field is expressed as

$$c_i(r) = c^o + \left(\frac{D_e c^o (R-\tau)}{D_e(R-\tau) + D_g \tau} - c^o \right) \left(\frac{R}{\tau} - \frac{R(R-\tau)}{r\,\tau} \right) . \qquad (9)$$

The evaporation rate is determined by substituting Eq.9 into Eq.3, i.e.,

$$\dot{v}_l = 4\pi\bar{v}_l R^2 D_e \frac{\partial c_i}{\partial r}\Big|_R = -\frac{4\pi\bar{v}_l R\,(R-\tau) D_e D_g c^o}{D_e(R-\tau) + D_g\tau} . \qquad (10)$$

Note that if $\tau=0$, Eq.10 reverts to the expression for pure droplet evaporation as expected. To integrate Eq.10, τ must be expressed as a function of time or as a function of the liquid volume v_l. Focusing on the shrinking core of radius R-τ, the volume of the core is expressed in terms of the solid and liquid volumes as

$$v_l + v_s = \frac{4\pi}{3}(R-\tau)^3 \qquad (11)$$

where v_l and v_s are the volumes of liquid and solid, respectively, within the shrinking core. The liquid is assumed to fill the interstitial volume and the pores of the primary particles. Rewritting Eq.11 and using the definition $v_s/v_l = 1/\epsilon\rho_s$, where ϵ and ρ_s are the total free volume (cc/gm) and solid density (gm/cc), respectively, the shell thickness is written as

$$\tau = R - \left(\frac{3(1+\epsilon\rho_s)}{4\pi\epsilon\rho_s} v_l\right)^{1/3} . \qquad (12)$$

Substituting Eq.12 into Eq.10, the liquid volume evaporation rate is given by

$$\dot{v}_l = -\frac{4\pi R\,\bar{v}_l\,c^o}{\frac{1}{D_g} - \frac{1}{D_e} + \left(\frac{4\pi\epsilon\rho_s R^3}{3(1+\epsilon\rho_s)\,D_e^3}\right)^{1/3} v_l^{-1/3}} . \qquad (13)$$

Using separation of variables, Eq.13 is readily integrated to give

$$\left(\frac{1}{D_g}-\frac{1}{D_e}\right)(v_l(t) - v_l(0)) + \frac{3}{2D_e} v_l(0)^{1/3}\left(v_l(t)^{2/3} - v_l(0)^{2/3}\right) = -4\pi R\bar{v}_l c^o t \qquad (14)$$

where

$$v_l(0) = \frac{4\pi R^3 \epsilon \rho_s}{3(1+ \epsilon\rho_s)} .$$

To compare the levitation voltage data to model predictions, the liquid volume v_l must be related to the levitation voltage V. Because the relative levitation voltage is equal to the relative particle mass, i.e.,

$$\frac{V(t)}{V(0)} = \frac{m_s + m_l}{m_s + m_l(0)}$$

then using Eqs.11 and 12, the relative levitation voltage is related to the liquid volume by the relation

$$\frac{V(t)}{V(0)} = \left(\frac{1 + \frac{3(1+ \epsilon\rho_s)\rho_l v_l}{4\pi R^3 \rho_s}}{1+ \epsilon\rho_l}\right). \qquad (15)$$

Thus, levitation voltages are calculated by first solving Eq.14 and then substituting the results into Eq.15. The following parameter values are used in the calculation: D_g=0.06 cm^2/sec; c^o=5.18x10^{-9} moles/cc; ρ_s=2.29 gm/cc; ρ_l=0.8270 gm/cc; and v_l=157.47 cc/mole. The gas phase diffusion coefficient D_g is computed using the molecular theory of gases for rigid sphere collisions (Rubel, 1984). The particle radius R at the onset of shrinking core evaporation is determined by noting the time at which the particle transforms from the wet to dry state and using the pure droplet flux rate (Eq.2) to evaluate the corresponding particle radius. The remaining parameters to be defined are the free volume ϵ and the shell diffusion coefficient D_e.

The free volume is determined from the levitation voltage of the octyl alcohol-saturated particle V_s (voltage at particle darkening) and the levitation voltage of the dry particle (v_l=0) using Eq.15. Setting v_l=0, the free volume is given by

$$\epsilon = \frac{V_s / V_D - 1}{\rho_l} \qquad (16)$$

where V_D is the levitation voltage of the dry particle. From Figs. 3a-c, the free volumes are found to be 3.26, 1.96, and 1.09 cc/gm for Syloids 244, 72, and 63, respectively. These results can be compared to the oil absorption data reported by W.R. Grace (Table 1) by converting the free volume to an oil weight equivalent. Because the oil absorption data is referenced to a dibutylphthalate liquid with a bulk density of 1.047 gm/cc, the free volume is converted to an oil weight equivalent by multiplying the free volume by the density factor 1.047. The oil weight equivalent based on the experimental data become 3.41, 2.05, and 1.14 for Syloids 244, 72, and 63, respectively. These oil absorption values compare favorably with the data in Table 1, i.e., 2.80, 2.20, 0.60.

Once the free volume is determined, the only remaining adjustable parameter is the effective shell diffusion coefficient D_e which is evaluated by a "best fit" between data and shrinking core model calculations. Figures 4a-c show model calculations for three different values of D_e for each of the three mixture silica particles. The value DE2 represents the "best fit" which is determined by calculating the correlation coefficient for the data-model pair. The value DE1 represents the case where the shell diffusion coefficient equals the gas phase coefficient, i.e., unhindered diffusion. The calculation with DE3 shows the sensitivity of the model on the value of the effective diffusion coefficient. Fig.4a shows the comparative fit for the evaporation of the Syloid 72 mixture particle. The normalized levitation voltage is referenced to the saturation voltage V_s. The best fit between data and model is obtained with DE2=0.019 cm^2/sec with a correlation coefficient of 0.994. A similar analysis is applied to the Syloid 244 evaporation data as shown in Fig.4b. Best fit is found for an effective diffusion coefficient equal to 0.025 cm^2/sec with a correlation coefficient of 0.997. For the Syloid 63 mixture particle, the "best fit" value for the diffusion coefficient is 0.015 cm^2/sec.

Thus the ranked order for the shell diffusion coefficient in descending order is 0.025 cm^2/sec, 0.019 cm^2/sec, 0.015 cm^2/sec for Syloids 244, 72, and 63, respectively. Qualtitatively the decrease in the diffusion coefficient with decreasing Syloid number is consistent with the porosity data shown in Table 1. Specifically, from Table 1 it is evident that the pore radius, which is proportional to the ratio of the pore volume to the surface area, decreases with decreasing Syloid number. By Knudsen flow considerations the shell diffusion coefficient is proportional to the pore radius and thus according to Table 1, the pore diffusion coefficient should decrease with decreasing Syloid number which is consistent with our results.

Quantitatively, the pore radius can be calculated from the experimental shell diffusion

coefficient using Wheeler's (1955) parallel pore model in combination with Knudsen capillary flow considerations. According to Wheeler's parallel pore model, the shell diffusion coefficient is related to the single pore diffusion coefficient D_p by the relation

$$D_e = \frac{\eta}{\kappa^2} D_p \qquad (17)$$

where η is the surface porosity of the shell and κ is the tortuosity factor describing the deviation of the pores from ideal cylinders. The surface porosity of the shell is defined as the ratio of the pore surface area to the shell surface area and ranges in value from 0 to 1. Without supporting data, the surface porosity is set arbitrarily at an average value of 0.5 for all Syloids. In the present calculation it is assumed that cylindrical geometry exists and that $\kappa=1$. If the capillary radius is much less than the mean free path of the gas, as is the case for the silicas, then diffusion through the capillary is described by Knudsen flow. The individual pore diffusion coefficient for a cylindrical pore is

$$D_p = \frac{4r_c}{3}\sqrt{\frac{2R_gT}{\pi M_w}} \qquad (18)$$

where r_c is the pore radius and M_w is the molecular weight of the diffusing gas. Then the pore radius can be determined from Eqs. 17 and 18 from knowledge of the effective diffusion coefficient and the surface porosity. Performing these calculations the pore radius is determined to be 374, 284, and 224 Å for Syloids 244, 72, and 63, respectively. Average pore sizes can be calculated from Table 1 using the pore radius expression given by Alishusky and Fournier (1990) $r_c = 4V_p/A_p$, where V_p and A_p are the pore volume and surface area, respectively. Using the values in Table 1, the literature values for the pore radii are 181, 47, and 24 Å for Syloids 244, 72, and 63, respectively.

It is evident that the present study overestimates the pore radii of the Syloids when compared to the porosity data of W.R.Grace. One possible explanation is the assumption that interstitial volume evaporation can be neglected is invalid. Because the evaporation flux from the interstitial volume is greater than that from the pore volume, the presence of interstitial volume will increase the best fit value for the effective diffusion coefficient. Consequently, the value of the pore radius is increased due to presence of interstitial evaporation. Further evidence for the contribution of interstitial evaporation is found in the primary particle diameter data given in Table 1. Because the aggregate with the largest primary particles possesses the largest interstitial volume, it is expected that Syloid 63 would show the greatest disparity in the pore radii and Syloid 244 would show the smallest. Indeed this is the case as disparties in the pore radii range from a factor of 2 for Syloid 244 to factor of 10 for Syloid 63.

Future efforts will be directed to developing a composite model which can account for combined interstitial and pore volume evaporation. This model will be applied to the present data to ascertain a more accurate estimate of the pore radii of the solids. Another approach is to measure the evaporation flux from microparticles composed of single primary particles. This would eliminate the presence of interstitial evaporation and would be amenable for analysis by the shrinking core evaporation model.

Conclusions

The evaporation of octyl alcohol from single microparticles composed of an aggregate of primary silica particles is measured using single particle electrical levitation. It is demonstrated that the evaporation flux is retarded by the porous silica particles and the evaporation retardation increases with decreasing silica pore size. A shrinking core evaporation model is developed that accounts for pore evaporation and effective diffusion coefficients are determined by comparing model results to data. Using Knudsen flow considerations, pore radii are evaluated from the diffusion coefficients and compared to literature data. It is found that the pore radii determined in the present study exceed literature values suggesting that interstitial evaporation (evaporation from the volume between the particles) is contributing to the microparticle evaporation rate. It is also demonstrated that single particle levitation can be used to determine the liquid absorption capacity of solid particles rapidly and accurately.

Table 1. Typical Physical and Chemical Characteristics of Syloid Silicas (W.R.Grace Chemical Co.)

Syloid	**63**	**72**	**244**
SiO_2(%)	99.4	99.4	99.4
Avg.Particle Size (μm)	9	4	3
Surface Area (m^2/gm)	675	340	310
Oil Absorption (lb/100lb)	60	220	280
Bulk Density (lb/ft^3)	29	11	8
Soluble Salts (%)	0.5	0.3	0.2
Pore Volume (cc/gm)	0.4	0.4	1.4

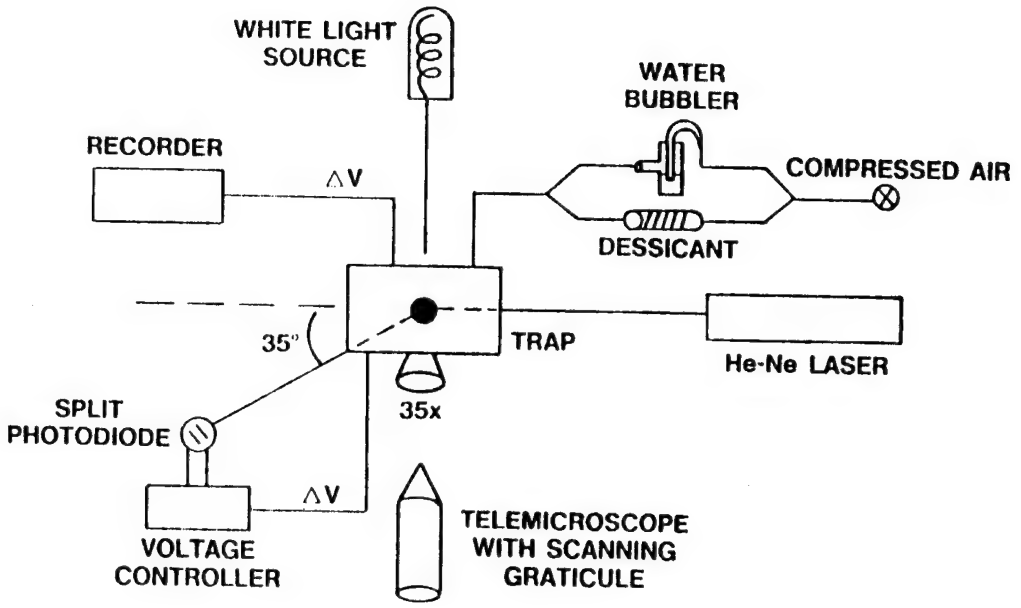

Figure 1. Schematic of Single Particle Electrodynamic Levitation (SPEL) Apparatus and Ancillary Gas Conditioning and Particle Detection Devices.

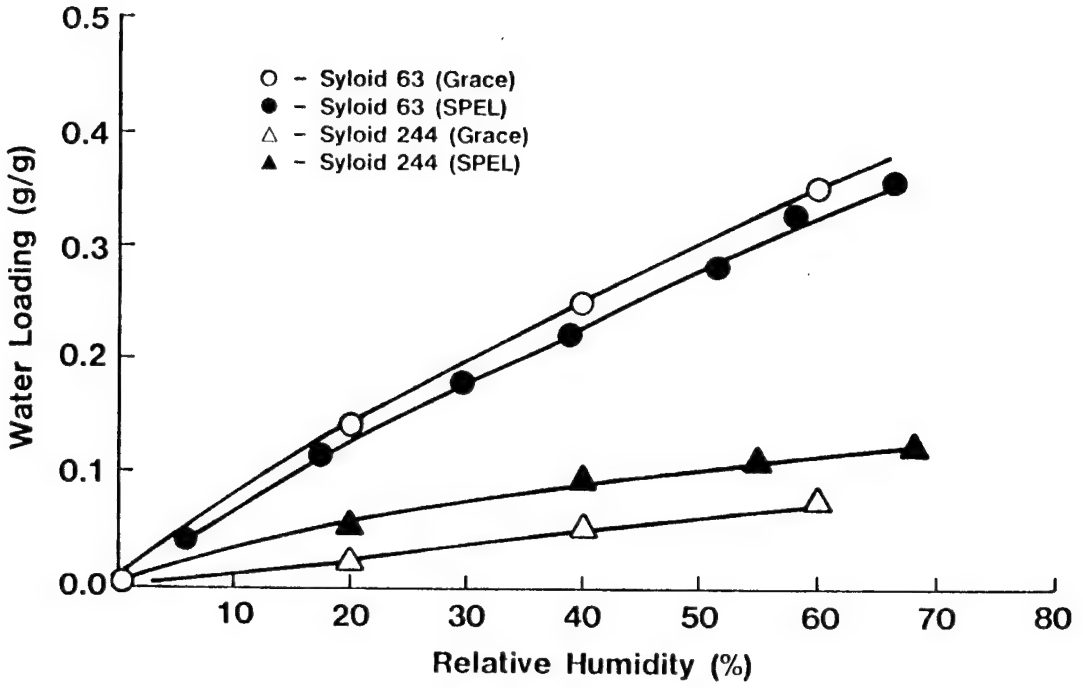

Figure 2. Comparison of Syloid Silica Water Isotherms as Measured by W.R. Grace for Bulk Samples and as Measured by SPEL for Single Particles.

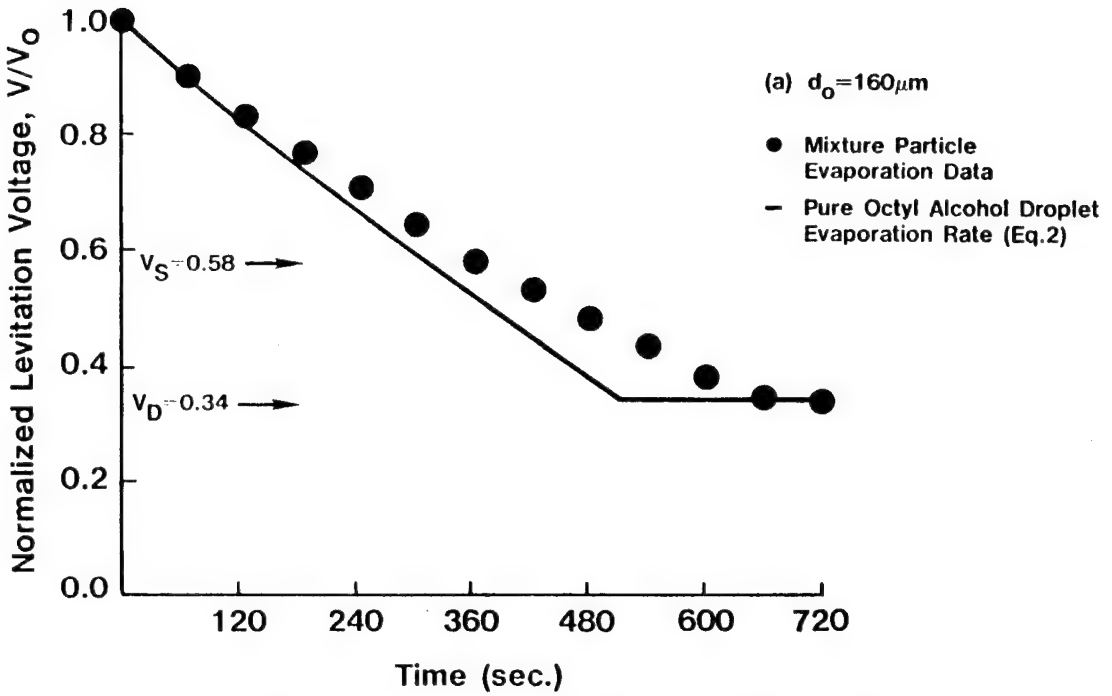

Figure 3a. Evaporation Data for a Mixture Particle Initially Composed of 38% Syloid 63 and 62% Octyl Alcohol and Calculated Evaporation Rate of an Octyl Alcohol Droplet with a Solid Core.

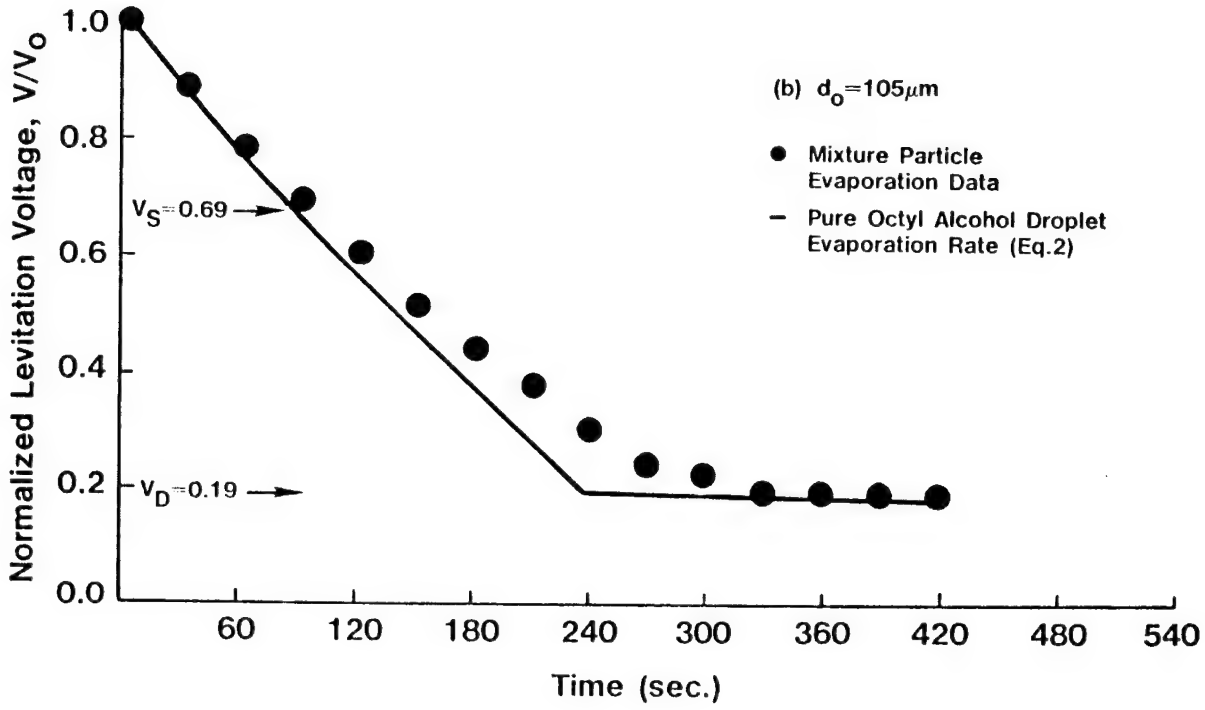

Figure 3b. Evaporation Data for a Mixture Particle Initially Composed of 22% Syloid 244 and 78% Octyl Alcohol and Calculated Evaporation Rate of an Octyl Alcohol Droplet with a Solid Core.

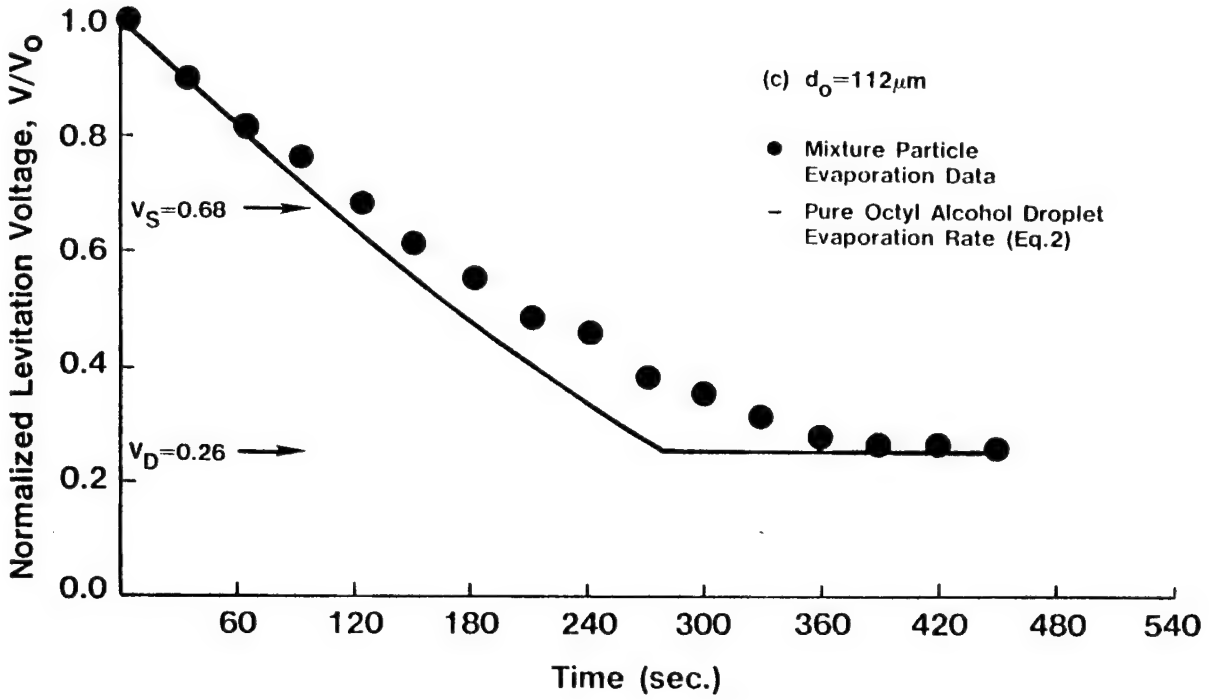

Figure 3c. Evaporation Data for a Mixture Particle Initially Composed of 25% Syloid 72 and 75% Octyl Alcohol and Calculated Evaporation Rate of an Octyl Alcohol Droplet with a Solid Core.

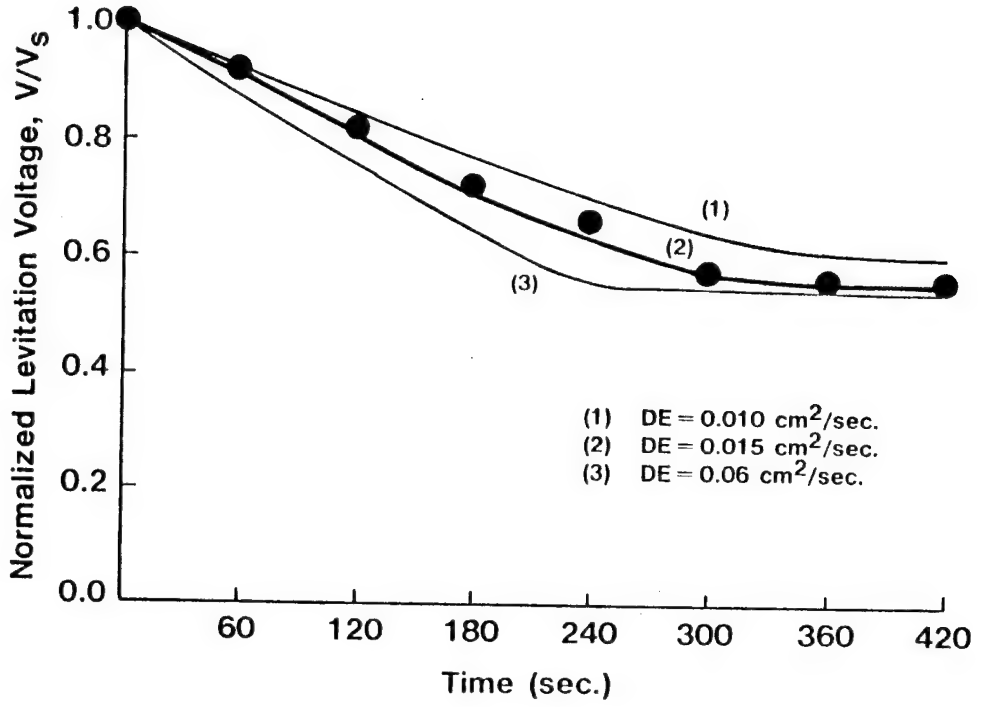

Figure 4a. Comparison of Evaporation Data for Mixture Particle Depicted in Fig.3a and Shrinking Core Evaporation Model Calculations for Three Values of the Effective Diffusion Coefficient DE. "Best fit" DE=0.015 cm^2/sec.

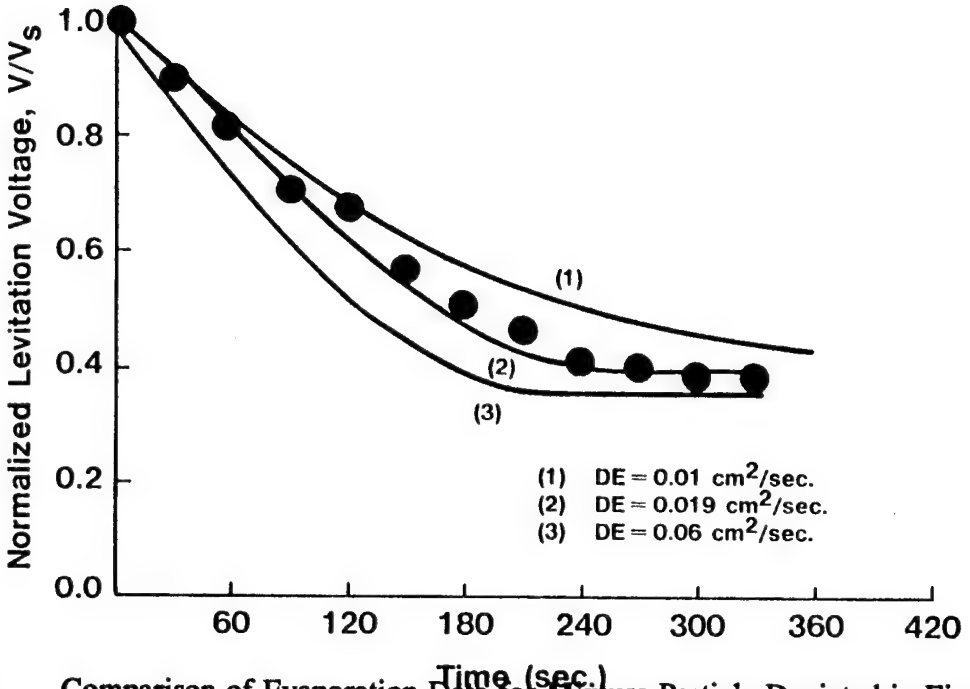

Figure 4b. Comparison of Evaporation Data for Mixture Particle Depicted in Fig.3b and Shrinking Core Evaporation Model Calculations for Three Values of the Effective Diffusion Coefficient DE. "Best fit" DE=0.019 cm^2/sec.

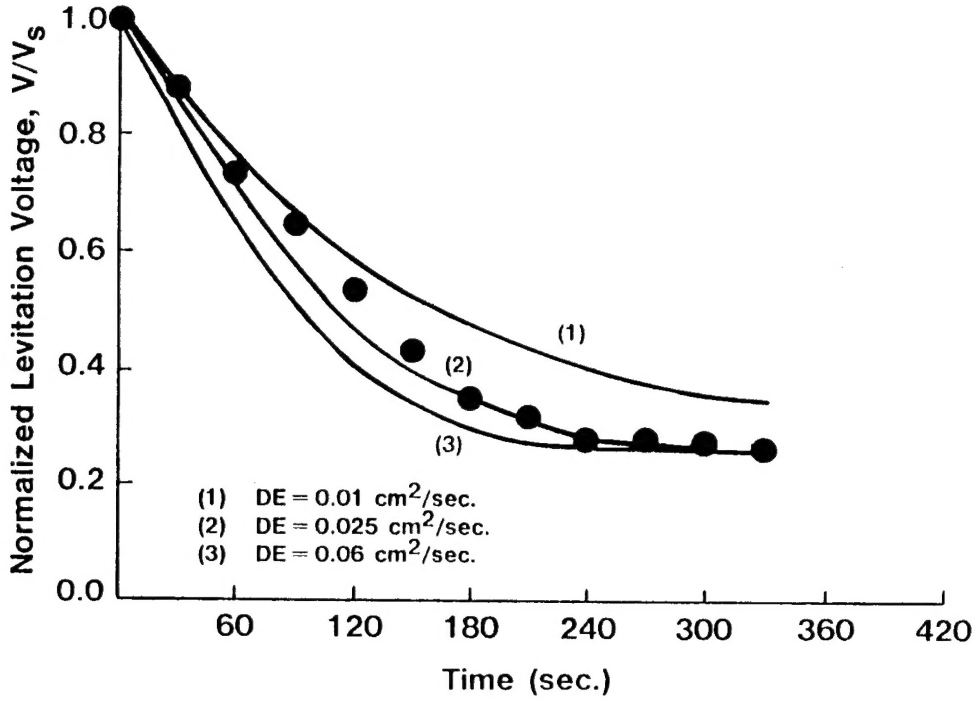

Figure 4c. Comparison of Evaporation Data for Mixture Particle Depicted in Fig.3c and Shrinking Core Evaporation Model Calculations for Three Values of the Effective Diffusion Coefficient DE. "Best fit" DE=0.025 cm^2/sec.

REFERENCES

Abramzon, B.M., A.A.Kossoi, and E.S.Ozerov, "Calculation of the Drying Rate of Particles of Porous Materials," *Advances in Aerosol Physics*, No.7, John Wiley & Sons, New York, 10 (1972).

Alishusky, J.J., and R.L.Fournier, "Partitioning and Adsorption of Aromatic Compounds on Microporous Silica Gel,"*AICHE J.*,**36**, 1605 (1990).

de Laplace, P.S., *Mechanique Celeste*, Supplement to Book 10, (1806).

Rubel, G.O., and M.E.Milham, "Determination of Vapor Pressure/Molecular Weight Correlations from Droplet Evaporation Data,"*Chem. Eng. Sci.*, **39**, 1043 (1984).

Rubel, G.O., "Reaction of Microparticles by the Diffusion of Reactive Gases through Porous Shells,"*J.Appl.Phys.*, **61**, 1633 (1987).

Wheeler, A., *Catalysis*, Vol.2, Reinhold, New York (1955).

Blank

Notations

c° = octyl alcohol saturation vapor concentration at temperature T (moles/cm^3)
c_{ex} = octyl alcohol vapor concentration external to particle (moles/cm^3)
c_i = octyl alcohol vapor concentration inside porous shell (moles/cm^3)
d = particle diameter (cm)
D_g = octyl alcohol gas phase diffusion coefficient (cm^2/sec)
D_e = porous shell diffusion coefficient (cm^2/sec)
D_p = pore diffusion coefficient (cm^2/sec)
m = particle mass (gm)
m_o = initial particle mass (gm)
m_s = silica mass (gm)
m_l = octyl alcohol liquid mass (gm)
M_W = octyl alcohol molecular weight (gm/mole)
N = a constant (moles/sec)
P_D = octyl alcohol partial pressure at droplet surface (ergs/cm^3)
P_∞ = octyl alcohol partial pressure at infinity (ergs/cm^3)
r = radial coordinate (cm)
r_c = pore radius (cm)
R = radius of solid particle (cm)
R_g = gas constant (ergs/mole-°K)
t = time (sec)
T = temperature (°K)
v_l = octyl alcohol volume (cm^3)
v_l = octyl alcohol molar volume (cm^3)
v_s = silica volume (cm^3)
V = levitation voltage (volts)
V_o = initial levitation voltage (volts)
V_D = dry particle levitation voltage (volts)
V_s = levitation voltage of octyl alcohol-saturated particle (volts)

Greek Letters

ϵ = free volume of particle (cm^3/gm)
κ = solid tortuosity
η = solid surface porosity
ρ_s = silica density (gm/cm^3)
ρ_l = octyl alcohol density (gm/cm^3)
τ = shell thickness (cm)